ISSN 1063-7729, Astronomy Reports, 2006, Vol. 50, No. 4, pp. 289–297. © Pleiades Publishing, Inc., 2006.
Published in Russian in Astronomicheskiĭ Zhurnal, 2006, Vol. 83, No. 4, pp. 327–336.

The Detection of Class I Methanol Masers towards Regions of Low-Mass Star Formation*

S. V. Kalenskiĭ[1], V. G. Promyslov[1], V. I. Slysh[1], P. Bergman[2], and A. Winnberg[2]

[1] *Astro Space Center, Lebedev Physical Institute, Moscow, Russia*

[2] *Onsala Space Observatory, Onsala, Sweden*

Received July 12, 2005; in final form, September 7, 2005

Abstract—Six young bipolar outflows in regions of low–intermediate-mass star formation were observed in the $7_0-6_1A^+$, $8_0-7_1A^+$, and $5_{-1}-4_0E$ methanol lines at 44, 95, and 84 GHz, respectively. Narrow features were detected towards NGC 1333-IRS4A, HH 25MMS, and L1157-B1. The flux densities of the detected lines are not higher than 11 Jy, which is much lower than the flux densities of strong maser lines in regions of high-mass star formation. Analysis shows that the narrow features are most likely masers.

PACS numbers : 98.38.E, 97.10.B
DOI: 10.1134/S1063772906040032

1. INTRODUCTION

Bright and narrow maser lines of methanol (CH_3OH) have been found towards many star-forming regions. According to the classification of Menten [1], methanol masers can be divided into two classes, I and II. Class I masers emit in the $7_0-6_1A^+$ transition at 44 GHz, $4_{-1}-3_0E$ transition at 36 GHz, $5_{-1}-4_0E$ transition at 84 GHz, etc., while the Class II masers emit in the $5_1-6_0A^+$ transition at 6.7 GHz, $2_0-3_{-1}E$ transition at 12 GHz, and in the $J_0-J_{-1}E$ series of transitions at 157 GHz, etc. Class II masers are often associated with ultra-compact HII regions or infrared sources. According to current views, Class I masers are collisionally pumped, while Class II masers are pumped by external radiation.

As a result of a number of surveys in the $7_0-6_1A^+$, $4_{-1}-3_0E$, $5_{-1}-4_0E$, etc. Class I lines, more than a hundred Class I masers have been found in high-mass star-forming regions. At the same time, Bachiller et al. [2] and Kalenskii et al. [3] did not find any masers towards low-mass stars in their observations of a large number of high-mass and low-mass young stars in the $7_0-6_1A^+$ line. Therefore, it is generally thought that the Class I masers are associated with massive stars. An exception is the detection by Kalenskii et al. [4] of a narrow probable maser feature in the $5_{-1}-4_0E$ and $8_0-7_1A^+$ Class I lines towards the blue wing of a bipolar outflow driven by the young low-mass star L1157-mm. The gas in this direction is shock heated to a temperature of about 100 K, and the abundance of methanol, ammonia, formaldehyde, and many other molecules are enhanced due to grain-mantle evaporation.

The reason for the nondetection of masers at 44 GHz by Bachiller et al. [2] and Kalenskii et al. [3] could be due to either insufficiently high sensitivity (about 10 Jy) or a poor choice of star-forming regions and/or observing positions. In particular, it is reasonable to assume that methanol masers are formed towards the *wings* of bipolar outflows, where the abundance of methanol is enhanced [5]. However, in the survey of Bachiller et al. [2], the telescope was often pointed towards IRS objects, and in the survey of Kalenskii et al. [3], it was pointed towards IRS objects almost without exception. IRS objects coincide spatially with the central sources of outflows rather than their wings. The low-mass objects that were observed in [2, 3] are located relatively close to the Sun, usually at a distance of less than 500 pc. Accordingly, regions where the gas is shock heated are often located approximately 1′ or more from the central sources. Masers associated with these regions would fall outside the 2′ main beam of the telescope used in [2, 3]. Regions of massive star formation are much rarer than regions of low-mass star formation. Most are located several kpc from the Sun, and their angular sizes are usually less than 1′. Therefore, the masers fall within the antenna beams in single-dish observations, and tend to be detected independently of their exact locations in the star-forming regions. For example, the masers in the relatively nearby (2 kpc from the Sun) region of massive star formation L379 are located towards the

*This text was submitted by the authors in English.

Table 1. Main parameters of the observed lines and of the telescope at the line frequencies

Transition	Frequency, GHz	Line strength*	HPBW**	Jy/K
$7_0-6_1A^+$	44.069476	2.8609	82″	20.5
$5_{-1}-4_0E$	84.521206	1.4115	44	22
$8_0-7_1A^+$	95.169516	3.3377	39	25
$2_{-1}-1_{-1}E$	96.739393	1.5	39	25
$2_0-1_0A^+$	96.741377	2	39	25
2_0-1_0E	96.744549	2	39	25
2_1-1_1E	96.755507	1.5	39	25

* From Lees et al. [8].
** Full half-power beamwidth.

wing of a bipolar outflow; however, they fell into the main beam of the telescope when the central source IRS 18265−1517 was observed [3]. The closest maser is 30″ from this object, which corresponds to a linear distance of 0.3 pc.[1)] If L379 were located 500 pc from the Sun, all angular distances would increase by a factor of four. The masers would be 120″ from the IRS object and would not fall into the telescope beam.

There are other regions where Class I masers are located far enough from IRS objects and bipolar-outflow centers that the angular distances between the masers and these objects would be larger than 60″ if the distances to the sources were not more than 200–500 pc. For example, the maser spots in W33Met are 0.7 pc away from the nearest known IR object, which would correspond to an offset of 287″ if the distance to the source were 500 pc. However, there are regions where the offsets of methanol masers from IRS objects or bipolar-outflow centers are small. For instance, the maser in M8E is located only 0.02 pc away from the center of a bipolar outflow [6], which, even at a distance as small as 200 pc, would correspond to an offset of only 23″. The Class I maser GGD 27 coincides spatially with the center of a bipolar outflow within the errors [7]. Therefore it is unlikely that Bachiller et al. [2] and Kalenskii et al. [3] failed to detect any masers towards low-mass stars, only because they observed mostly IRS objects; it may be that the sensitivity of these surveys was insufficient as well.

The detection of methanol masers in relatively nearby sources could be very important for maser studies. Therefore, we observed several nearby bipolar outflows from low-mass stars in the $7_0-6_1A^+$ line at 7 mm, as well as in the $5_{-1}-4_0E$ line, $8_0-7_1A^+$ line, and the 2_K-1_K series of lines at 3 mm.[2)] The lines in this series are purely thermal and never exhibit maser emission. Several objects with enhanced methanol abundances were selected as targets.

2. OBSERVATIONS

The observations were performed with a 20-m radio telescope of the Onsala Space Observatory (Sweden). The line frequencies, strengths, and the main parameters of the telescope are presented in Table 1. A dual-beam switching mode with a frequency of 2 Hz and a beam throw of 11′ was applied. Pointing errors were checked using observations of SiO masers and found to be within 5″. The data were calibrated using a chopper-wheel method. The data were reduced with the CLASS package. The line rest frequencies were taken from the database of Lovas.[3)]

Observations in the $7_0-6_1A^+$ line were carried out on December 6–9, 2004. The main beam efficiency was about 0.5 for elevations lower than 30° and about 0.56 for elevations higher than 30°. The half-power beamwidth was 82″. The system noise temperature corrected for atmospheric absorption, rearward spillower, and radome losses varied between 180 and 400 K. An autocorrelator with a 12.5 kHz resolution (0.085 km/s at 44 GHz) was used as the spectrometer.

Observations in the 3-mm wave range were carried out in May 2001. The main beam efficiency and the half-power beamwidth at 84.5 GHz were 0.6″ and 44″, respectively. A cryogenically cooled low-noise SIS mixer was used. The system noise temperature corrected for atmospheric absorption, rearward spillower, and radome losses varied between 300 and 1000 K. The backend consisted of an autocorrelator with a 50 kHz resolution (0.177 km/s at 84.5 GHz); in parallel, a 256-channel filter spectrometer with a 250 kHz resolution (0.887 km/s at 84.5 GHz) was connected.

3. RESULTS

The results are presented in Figs. 1 and 2 and in Tables 2 and 3. Emission at 7 mm was detected in all six observed regions. Narrow features were found towards NGC 1333-IRS4A, HH 25MMS, and L1157-B1. The antenna temperatures of the detected lines do not exceed 0.52 K, which corresponds to a flux density of 10.7 Jy. Thus, the detected lines are

[1)] For simplicity, we call "distance" the projected distance in the plane of the sky.

[2)] The observations at 3 mm are part of a more extended survey, the results of which will be published elsewhere.

[3)] http://physics.nist.gov/cgi-bin/micro/table5/start.pl.

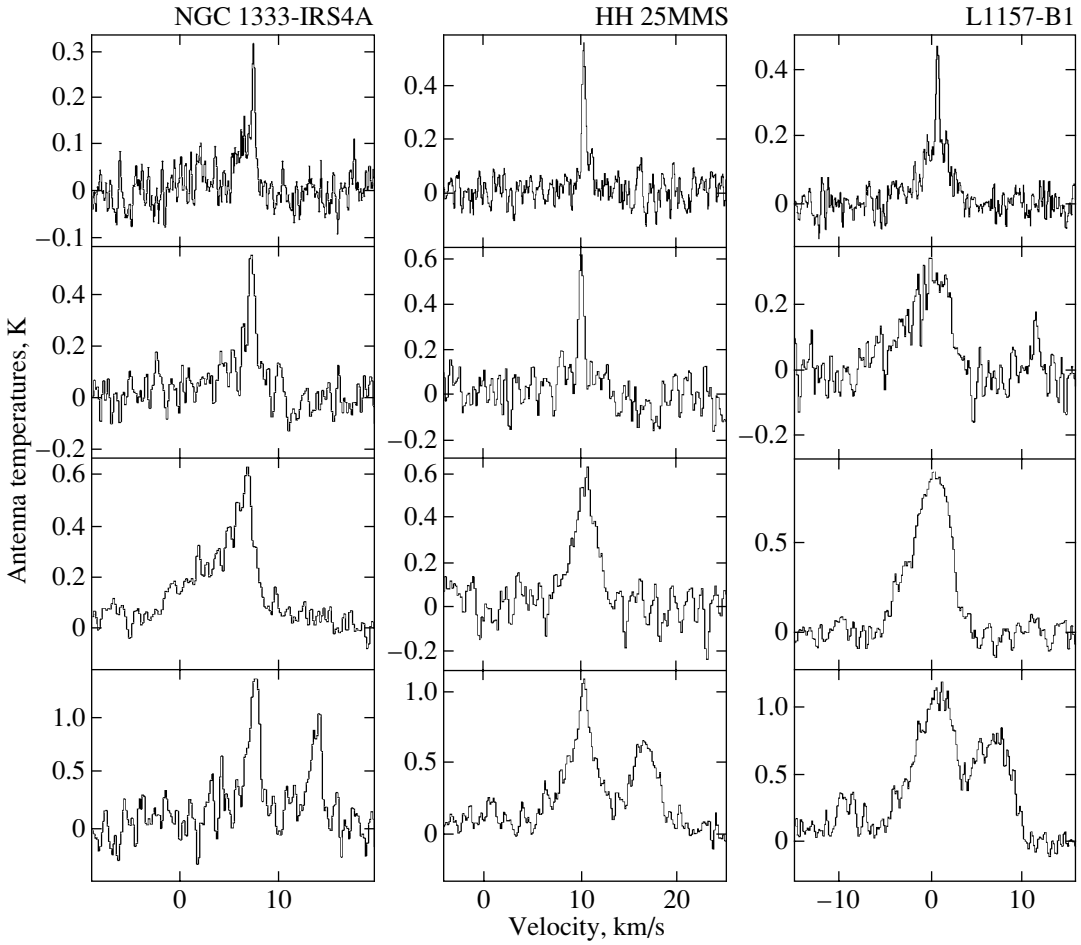

Fig. 1. Spectra of sources in which masers in the $7_0-6_1A^+$ line were detected. Shown from top to bottom are the $7_0-6_1A^+$, $8_0-7_1A^+$, $5_{-1}-4_0E$, and 2_K-1_K lines. The horizontal axis plots the radial velocity in km/s and the vertical axis the antenna temperature in Kelvin.

much weaker than the strong maser lines in massive star-forming regions, which have flux densities up to several hundred Janskys. In addition, the flux densities of the detected lines are approximately equal to or below the upper limits for the surveys of Bachiller et al. [2] and Kalenskii et al. [3]. Thus, the fact that no methanol maser emission in the $7_0-6_1A^+$ line was detected in [2, 3] can be fully or partially explained by the insufficient sensitivity of these surveys.

We observed several regions in the molecular cloud NGC 1333, where low-to-intermediate-mass stars are actively forming. A narrow feature at 44 GHz was detected towards the infrared source IRS4A. Figure 3 shows that both the central source and the peaks of CO emission in the red and blue wings of the outflow fall into the antenna beam. Therefore, without additional observations with high spatial resolution we cannot determine with which of these objects the narrow feature is related. Blake et al. [9] found that the abundances of CS, SiO, and CH_3OH toward this source are enhanced due to grain-mantle evaporation. In this same direction, we detected features at 84 and 95 GHz that are broader than the narrow feature at 44 GHz, but narrower than the thermal lines at 96 GHz (Fig. 1); these features are probably masers whose optical depths, and consequently the degree of line narrowing, are lower than at 44 GHz.

Narrow lines at 44 and 95 GHz were detected towards the red wing of bipolar outflow in the dark cloud L1630 containing the central source HH 25MMS, which is located to the south of the IR source IRS 05435−0014 (Fig. 4). A broad line was found at 84 GHz, whose width is close to those of the 2_K-1_K thermal lines. A high methanol abundance was detected in this direction by Gibb and Davis [10].

A narrow feature at 44 GHz is also detected towards the region B1 in the blue wing of the bipolar outflow, which is driven by the class 0 object (according to the classification of Andre et al. [11]) L1157-mm in the molecular cloud L1157 (Fig. 5). The abundances of methanol, ammonia, and a number of other molecules are enhanced in B1 due to

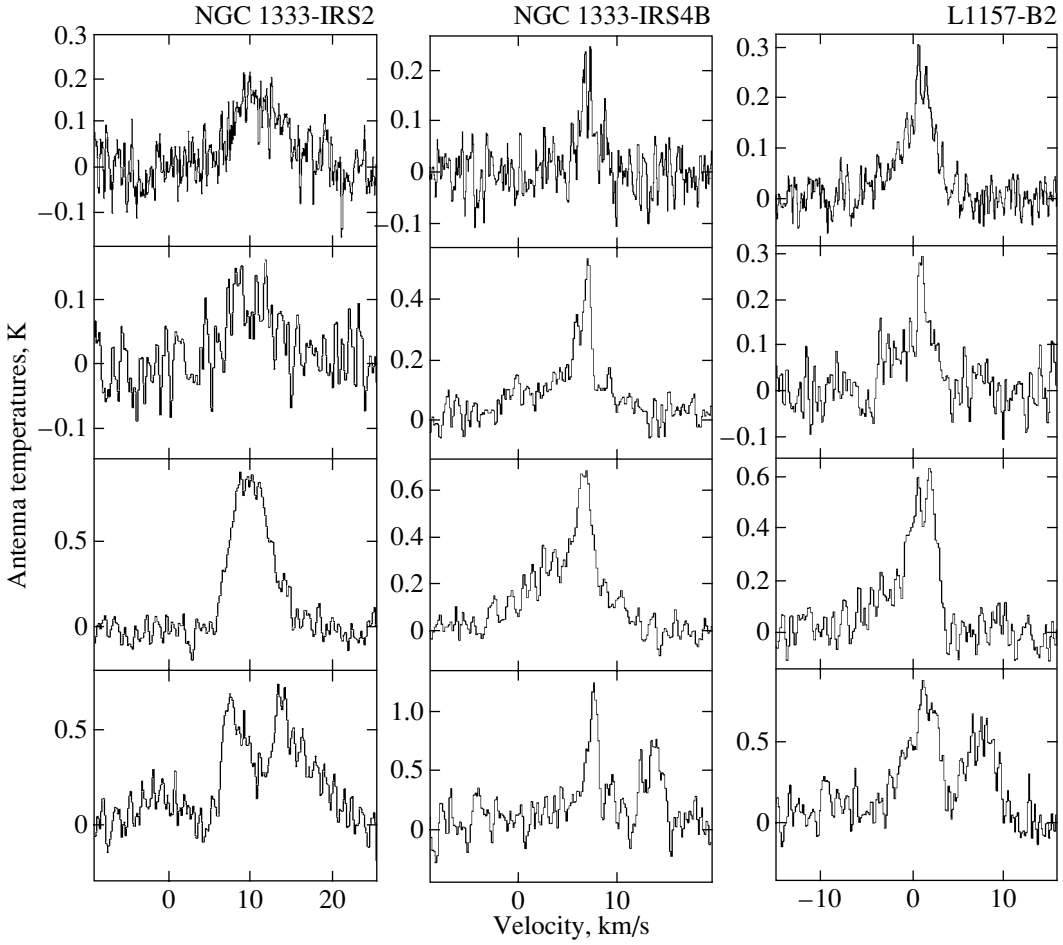

Fig. 2. Spectra of sources in which only thermal emission was detected. The spectra of L1157-B2 at 84 and 95 GHz are taken from [4]. The order of the lines and the horizontal and vertical axes are the same as in Fig. 1.

grain-mantle evaporation [12]. Only broad quasithermal lines were detected towards this region, at both 84 and 95 GHz (Fig. 1).

A narrow feature detected at 7 mm in the region B2, which is offset about 30″ from B1 (Fig. 5), is very weak; moreover, its radial velocity is the same as that of the narrow feature in B1. It is likely that there are no narrow lines related to B2, and that it is the narrow feature related to B1 that fell into the antenna beam, since its width is 82 arcsec.[4)]

4. DISCUSSION

The typical widths of thermal lines towards regions of high-mass star formation are about 3–5 km/s or higher. Therefore, a feature that is detected in a "maser" transition and is narrower than 1 km/s can be considered to be a maser without any additional justification. The situation in regions of low-to-intermediate mass star formation is different. The widths of the thermal lines of the quiescent gas in these regions are often 0.2–0.3 km/s or less. Therefore, the fact that a detected line is narrow does not necessarily mean that it represents a maser. Additional interferometric observations to measure the line brightness temperature are necessary.

An important argument that the detected narrow features are masers is that these features are observed in the $7_0-6_1A^+$ and $8_0-7_1A^+$ transitions, which have upper-level excitation temperatures E_u/k of 65 K and 84 K, respectively. The kinetic temperature of the quiescent gas in these regions is about 10–20 K; therefore, thermal excitation of these transitions in the quiescent gas is unlikely. These levels may be thermally excited in gas that has been heated and accelerated by shocks; however, the widths of thermal lines arising in such gas should vary from several km/s to several dozen km/s.

[4)]We cannot verify this hypothesis using the ratio of the observed intensities of the narrow features in B1 and B2, since we do not know the accurate position of the source observed in B1.

Table 2. Gaussian parameters of observed single lines

Source	RA (B1950) DEC (B1950)	Transition*	$\int T_A^* dV$, K km/s	$V_{\rm LSR}$, km/s	FWHM, km/s	T_A^*, K
NGC 1333-IRS2	$03^h25^m54.5^s$	I	1.33(0.06)**	10.83(0.17)	7.88(0.45)	0.16
	31°04′00″	II	0.98(0.08)	9.97(0.28)	8.38(0.85)	0.11
		III	5.32(0.09)	10.14(0.04)	5.46(0.10)	0.92
NGC 1333-IRS4A	03 26 04.8	I	0.16(0.02)	6.65(0.13)	1.59(0.22)	0.095
	31 03 13	I	0.09(0.02)	7.51(0.02)	0.33(0.05)	0.25
		II	1.01(0.11)	4.38(0.78)	8.93(1.49)	0.11
		II	0.44(0.06)	7.32(0.03)	0.94(0.14)	0.45
		III	1.60(0.12)	3.78(0.16)	7.19(0.31)	0.21
		III	0.16(0.04)	6.95(0.04)	0.67(0.13)	0.23
		III	0.64(0.03)	6.42(0.10)	2.31(0.17)	0.26
NGC 1333-IRS4B	03 26 06.5	I	0.32(0.03)	7.10(0.07)	1.83(0.21)	0.16
	31 02 51	II	1.15(0.07)	5.36(0.30)	9.31(0.57)	0.12
		II	0.16(0.04)***	6.08(0.07)	0.76(0.20)	0.20
		II	0.33(0.03)	7.16(0.04)	0.76(0.08)	0.40
		III	2.70(0.09)	4.72(0.15)	8.77(0.29)	0.29
		III	0.73(0.05)	6.86(0.04)	1.59(0.10)	0.43
HH 25MMS	05 43 34.0	I	0.27(0.02)	10.42(0.01)	0.48(0.04)	0.52
	−00 15 20	II	0.81(0.11)	9.97(0.36)	5.60(0.80)	0.14
		II	0.31(0.04)	10.14(0.03)	0.53(0.06)	0.54
		III	1.63(0.08)	10.53(0.07)	2.87(0.17)	0.53
L1157-B1	20 38 41.0	I	0.60(0.03)	0.69(0.08)	3.82(0.24)	0.17
	67 50 33	I	0.12(0.01)	0.75(0.01)	0.37(0.03)	0.31
		II	1.61(0.09)**	−0.18(0.15)	5.19(0.33)	0.29
		III	4.61(0.07)**	0.10(0.04)	4.81(0.09)	0.90
L1157-B2	20 38 42.2	I	0.61(0.09)	0.04(0.38)	5.29(0.43)	0.11
	67 50 03	I	0.28(0.11)***	1.53(0.14)	2.17(0.49)	0.12
		I	0.04(0.01)***	0.72(0.03)	0.36(0.08)	0.11

* Notation for line transitions: I, 7_0–6_1A^+; II, 8_0–7_1A^+; III, 5_{-1}–4_0E.
** Lines have non-Gaussian shape, but a fit using two or more components is not reliable.
*** Detection at the sensitivity limit.

Table 3. Gaussian parameters for lines in the 2_K-1_K series (Gaussian approximation of the lines assumes that the widths and radial velocities of all lines are the same)

Source	T_A^*, K				V_{LSR}, km/s	FWHM, km/s
	$2_{-1}-1_{-1}E$	$2_0-1_0A^+$	2_0-1_0E	2_1-1_1E		
NGC 1333-IRS2	0.45(0.03)	0.42(0.02)	0.15(0.02)	<0.06	9.51(0.14)	5.56(0.16)
	0.30(0.03)	0.41(0.03)	<0.09		7.53(0.05)	1.42(0.06)
NGC 1333-IRS4A	0.25(0.05)	0.37(0.05)	0.09(0.04)	<0.10	6.22(0.29)	5.31(0.37)
	0.79(0.07)	1.04(0.07)	<0.20		7.69(0.03)	1.14(0.04)
NGC 1333-IRS4B	0.58(0.07)	0.90(0.09)	<0.21		7.74(0.07)	1.24(0.07)
HH 25MMS	0.51(0.02)	0.76(0.03)	0.13(0.02)	<0.06	10.25(0.05)	3.56(0.07)
L1157-B1	0.75(0.02)	1.10(0.02)	0.28(0.02)	<0.06	0.43(0.05)	5.00(0.05)
L1157-B2	0.55(0.02)	0.75(0.02)	0.17(0.02)	<0.06	1.30(0.06)	4.00(0.07)

In order to quantitatively verify this argument, we modeled the narrow features detected in NGC 1333-IRS4A, HH 25MMS, and L1157-B1. For this purpose, we computed a grid of LVG models spanning 10–200 K in temperature, $0.32\times10^4-1.0\times10^8$ cm^{-3} in density, and $0.1\times10^{-4}-0.56\times10^{-1}$ cm^{-3}/(km/s/pc) in methanol density divided by the velocity gradient. We utilized the collisional decay rates for methanol derived in the quantum-mechanical calculations of Pottage et al. [13]. The agreement between the models and observational data was estimated using χ^2 criterion, with the values χ^2 calculated using the formula

$$\chi^2=\sum_I\left(\frac{R^I_{\rm obs}-R^I_{\rm mod}}{\sigma_{R^I_{\rm obs}}}\right)^2, \qquad (1)$$

where $R^I_{\rm obs}$ and $R^I_{\rm mod}$ are the observed and model flux-density ratios for the narrow features in the $7_0-6_1A^+$, $8_0-7_1A^+$, and $5_{-1}-4_0E$ lines, and $\sigma_{R^I_{\rm obs}}$ are the errors of the observed ratios. For HH 25MMS, we found that a number of models with $T_{\rm kin}\geq95$ K, 5.6×10^4 cm$^{-3}\leq n_{\rm H_2}\leq1.8\times10^5$ cm^{-3}, and a specific column density of methanol $N_{CH_3OH}/\Delta V$ of the order $10^{15}-10^{16}$ cm^{-2}/(km/s) satisfactorily reproduce the observed ratios. In all acceptable models, the $5_{-1}-4_0E$, $8_0-7_1A^+$, and $7_0-6_1A^+$ lines are inverted, with the absolute values of optical depths of the $5_{-1}-4_0E$ and $8_0-7_1A^+$ lines being comparable to or higher than 3, and those of the $7_0-6_1A^+$ line being comparable to or higher than 5. The brightness temperatures of the $5_{-1}-4_0E$ and $8_0-7_1A^+$ lines in the acceptable models vary from several hundred to several thousand Kelvin, while the brightness temperature of the $7_0-6_1A^+$ line is higher than 1000 K.

In the case of NGC 1333-IRS4A, an agreement was obtained for a number of models with $T_{\rm kin}\geq45$ K, 5.6×10^4 cm$^{-3}\leq n_{\rm H_2}\leq3.2\times10^5$ cm^{-3}, and $N_{CH_3OH}/\Delta V\approx10^{15}-10^{16}$ cm^{-2}/(km/s). The $5_{-1}-4_0E$, $8_0-7_1A^+$, and $7_0-6_1A^+$ lines were again inverted in all the acceptable models. The absolute values of optical depths of these lines vary from 3 to 5, while the brightness temperature varies from several hundred to several thousand Kelvin.

We failed to find any acceptable model for L1157-B1, since the intensities at 84 and 95 GHz corresponding to the intensity of the narrow feature at 44 GHz are above the upper limits presented in Table 2 in all the computed models. There are several explanations for this inconsistency in the framework of the maser hypothesis. For example, Sobolev et al. [14] suggested that compact masers arise in turbulent media, due to the fact that, in a turbulent velocity field, the coherence lengths along some directions are larger than the mean coherence length. If the masers are unsaturated, the intensity of maser emission is proportional to $\exp(-\tau)$, where τ is the optical depth along the direction toward the maser. To first approximation, we can suppose that LVG modeling yields the opacity averaged over all directions and the "mean" line brightness corresponding to this opacity. The larger the mean line opacity, the higher the ratio of the maximum to the mean brightness. Consider the case when the coherence length along some direction is twice its mean value. If the mean opacity is -5, which corresponds to the typical opacity of the $7_0-6_1A^+$ line, derived from modeling for HH 25MMS, then the ratio of the peak to the mean opacity is 2, and the peak opacity is -10. The ratio of the peak brightness temperature (i.e., the brightness temperature of the maser spot) to the mean brightness temperature (i.e., the model

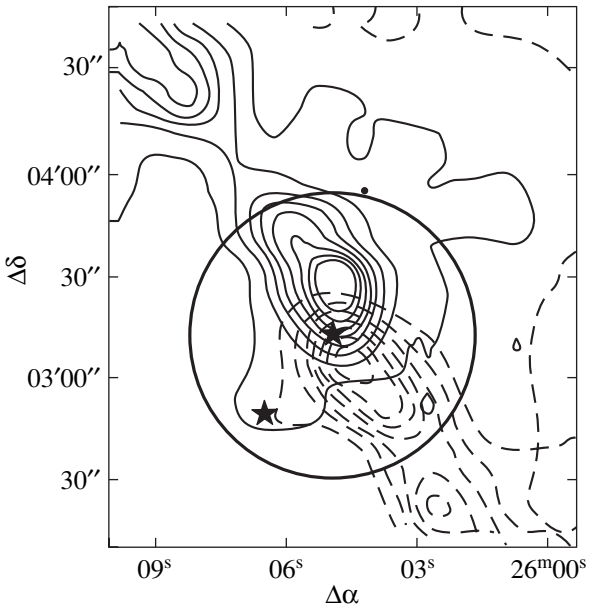

Fig. 3. Map of the environment of the IR source IRS4A in the cloud NGC 1333. The solid and dashed contours show the red and blue wings of the bipolar outflow (from [9]). The circle 82″ in diameter shows the size and position of the main beam of the telescope during the observations at 7 mm. The stars denote the sources IRS4A (at the center of the circle) and IRS4B (to the southwest of IRS4A).

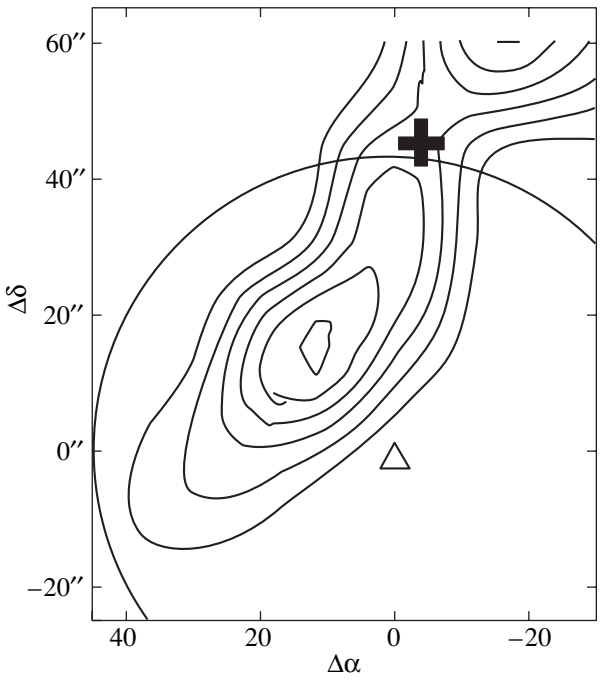

Fig. 4. Map of the environment of the submm source HH 25MMS. The solid contours show the red wing of the bipolar outflow in the $J = 3–2$ CO line (from [10]); the central star is denoted by a cross. The semicircle with the triangle at its center shows the size and position of the main beam of the antenna during the observations at 7 mm. The horizontal and vertical axes plot the offsets in the right ascension and declination (in arcsec) from the coordinates presented in Table 2.

brightness temperature) is $\exp(10)/\exp(5) \approx 150$. When the mean opacity is -3, which corresponds to the typical opacities of the $8_0–7_1A^+$ and $5_{-1}–4_0E$ lines, the ratio of the brightness temperature of the maser spot to the model brightness temperature is $\exp(6)/\exp(3) \approx 20$. Thus, in this example, the ratio of the brightness temperatures of the maser spots in the $8_0–7_1A^+$ and $5_{-1}–4_0E$ lines to the brightness temperature in the $7_0–6_1A^+$ line is less than the model ratio of the intensities of these lines by a factor of 7.5. This difference is sufficiently large to explain the nondetection of maser features in the $8_0–7_1A^+$ and $5_{-1}–4_0E$ lines in L1157-B1. Increasing the scatter of the coherence lengths can lead to much greater differences between the observed and model ratios of the line intensities.

It is interesting that Kalenskii et al. [4] observed narrow features at 95 GHz and probably 84 GHz towards the region B2, located 30″ from B1, in 2000, whereas we found only a very weak narrow feature at 7 mm towards this region in 2004; moreover, this feature may be related to B1 rather than to B2 (see above). To our knowledge, no Class I maser sources with a weaker emission at 44 GHz than at 84 and 95 GHz have been found. It is likely that Kalenskii et al. [4] observed a variable maser, whose intensity had substantially decreased by December 2004. Variability of at least two Class I maser sources, W3(OH) and G11.94-0.62, has been noted by Kurtz et al. [15]. Another possible explanation is that the 44-GHz maser is linearly polarized, and its plane of polarization was orthogonal to the plane of polarization of the receiver during the 2004 observations. No linear polarization has been detected from $7_0–6_1A^+$ masers, but linear polarization has been detected by Wiesemeyer et al. [16] in the $5_{-1}–4_0E$, $8_0–7_1A^+$, and $6_{-1}–5_0E$ lines, with the degree of the polarization in the $6_{-1}–5_0E$ line reaching 33–39%. It is likely that the degree of polarization in the stronger $7_0–6_1A^+$ line is the same or even higher, and can strongly affect the measured flux density.

It is interesting that the radial velocities of the maser features virtually coincide with those of the peaks of the $2_K–1_K$ thermal lines, which, in turn, are close to the radial velocities of the quiescent gas. The interferometric observations of L1157 in the CO and SiO lines of Gueth et al. [17, 18] revealed hollow shells, which they related to shock waves. It is reasonably to suppose that the methanol abundance is enhanced in these shells. The brightest masers should arise in the directions with the maximum opacity,

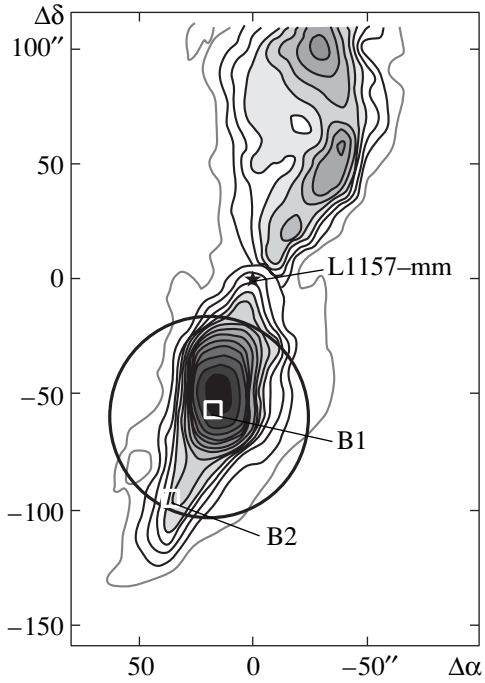

Fig. 5. The vicinity of the submm source L1157-mm. The map of the bipolar outflow is taken from Bachiller and Perez Gutierrez [12]. The circle with its center at B1 shows the size and position of the main antenna beam during the 7 mm observations. The horizontal and vertical axes plot the right ascension and declination offsets (in arcsec) from the coordinates ($J2000$) $\alpha = 20^{\rm h}39^{\rm m}06\overset{\rm s}{.}19$, $\delta = 68^\circ02'15\overset{''}{.}9$.

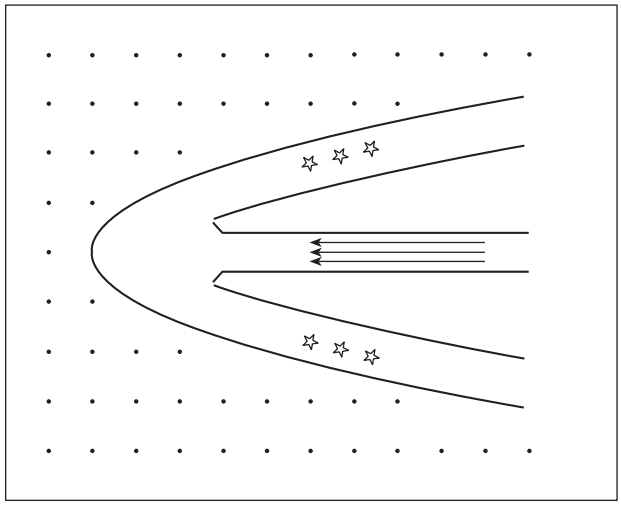

Fig. 6. A section of a bipolar outflow wing in the plane perpendicular to the observer. The stars denote the possible positions of methanol masers. The high-velocity jet (denoted by arrows) and the shell that appear behind the shock front are located between the solid lines. The points denote the quiescent gas.

i.e., along the walls, and should therefore be observed towards the positions indicated in Fig. 6. Since the gas parameters probably vary with position, the maser region should occupy only a small part of the shell. Since the outflow axis is nearly perpendicular to the observer, the radial velocity of the maser emission should be close to the radial velocity of the molecular cloud. This model, as well as the turbulence model noted above, supposes a preferential increase in the brightness of the most intense lines relative to the brightness ratios for various lines obtained for a uniform source of the same temperature and density. Testing this model requires interferometric observations at 44 GHz, first and foremost, of L1157, to compare the results with available interferometric maps in other molecular lines.

Thus, further interferometric observations are necessary, both to test whether the detected narrow lines are actually masers and to distinguish between different maser models. The detection of Class I methanol masers in relatively nearby regions of low-mass star formation can have a strong impact on the studies of these masers. On the whole, regions of low-mass star formation are much closer to the Sun and are much better studied than regions of high-mass star formation. Therefore, it is much easier to identify the observed masers with other objects (e.g., with the wings of bipolar outflows) than in observations of regions of high-mass star formation.

5. CONCLUSIONS

In observations taken during a short survey of bipolar outflows driven by low-mass young stars in the $7_0-6_1A^+$, $8_0-7_1A^+$, and $5_{-1}-4_0E$ methanol lines, we detected narrow features towards NGC 1333-IRS4A, HH 25MMS, and L1157-B1. The flux densities of these features are no higher than 11 Jy, which is much lower than the flux densities of strong maser lines in regions of high-mass star formation. Nevertheless, the narrow features are most likely masers. To confirm this requires further interferometric observations; these observations may also help distinguish between different maser models.

ACKNOWLEDGMENTS

The authors are grateful to the staff of the Onsala Space Observatory for help during the observations and to A.M. Sobolev for helpful discussions. This work was partially supported by the Russian Foundation for Basic Research (project nos. 01-02-16902 and 04-02-17057) and the Scientific Research Program of the Russian Academy of Sciences “Extended Sources in the Universe.” The Onsala Space Observatory is the Swedish National Facility for Radio Astronomy and is operated by Chalmers University of

Technology, Göteborg, Sweden, with financial support from the Swedish Research Council and the Swedish Board for Technical Development.

REFERENCES

1. K. M. Menten, in *Proceedings of the 3rd Haystack Observatory Meeting "Skylines,"* Ed. by A. D. Haschick and P. T. P. Ho, Astron. Soc. Pac. Conf. Ser. **16**, 119 (1991).
2. R. Bachiller, K. M. Menten, J. Gomez-Gonzalez, and A. Barcia, Astron. Astrophys. **240**, 116 (1990).
3. S. V. Kalenskii, R. Bachiller, I. I. Berulis, et al., Astron. Zh. **69**, 1002 (1992) [Sov. Astron. **36**, 517 (1992)].
4. S. V. Kalenskii, V. I. Slysh, I. E. Val'tts, et al., Astron. Zh. **78**, 31 (2001) [Astron. Rep. **45**, 26 (2001)].
5. R. L. Plambeck and K. M. Menten, Astrophys. J. **364**, 555 (1990).
6. I. E. Val'tts, Astron. Zh. **76**, 189 (1999) [Astron. Rep. **43**, 157 (1999)].
7. V. I. Slysh, I. E. Val'tts, S. V. Kalenskii, and V. V. Golubev, Astron. Zh. **76**, 892 (1999) [Astron. Rep. **43**, 785 (1999)].
8. R. M. Lees, F. J. Lovas, W. H. Kirchhoff, and D. R. Johnson, J. Phys. Chem. Ref. Data **2**, 205 (1973).
9. G. A. Blake, G. Sandell, E. F. van Dishoeck, et al., Astrophys. J. **441**, 689 (1995).
10. A. G. Gibb and C. J. Davis, Mon. Not. R. Astron. Soc. **298**, 644 (1998).
11. P. Andre, D. Ward-Thompson, and M. Barsony, Astrophys. J. **406**, 102 (1993).
12. R. Bachiller and M. Pérez Gutiérrez, Astrophys. J. **487**, L93 (1997).
13. J. T. Pottage, D. R. Flower, and S. L. Davis, J. Phys. B **37**, 165 (2004).
14. A. M. Sobolev, W. D. Watson, and V. A. Okorokov, Astrophys. J. **590**, 333 (2003).
15. S. Kurtz, P. Hofner, and C. V. Alvarez, Astron. J. **155**, 149 (2005).
16. H. Wiesemeyer, C. Thum, and C. M. Walmsley, Astron. Astrophys. **428**, 479 (2004).
17. F. Gueth, S. Guilloteau, and R. Bachiller, Astron. Astrophys. **307**, 891 (1996).
18. F. Gueth, S. Guilloteau, and R. Bachiller, Astron. Astrophys. **333**, 287 (1998).